Jurnal Tribologi 40 (2024) 78-94

MYTRIBOS Malaysian Tribology Society

Jurnal Tribologi

Website : jurnaltribologi.mytribos.org e-issn: 2289-7232

Effect of multi-geometrical laser pattern of Ti6Al4V on frictional wear behaviour

Mohd Harizan Zul [1], Mahadzir Ishak [1*], Ramdziah Md Nasir [2], Aiman Mohd Halil [2], Moinuddin Mohammed Quazi [2]

[1] Faculty of Mechanical and Automotive Engineering Technology, Universiti Malaysia Pahang, MALAYSIA.
[2] School of Mechanical Engineering, Universiti Sains Malaysia, MALAYSIA.
*Corresponding author: mahadzir@ump.edu.my

KEYWORDS

Ti6Al4V
Laser texturing
Multi-geometrical pattern
Wear
Friction

ABSTRACT

This research paper aims to investigate the impact of multi-geometrical patterns resulting from laser texturing of Ti6Al4V on friction and wear characteristics. The methodology involved laser texturing of the Ti6Al4V material with a laser power of 12 W, laser frequency of 40 kHz, and a laser scan speed of 180 mm/s. A frictional sliding wear test was performed using reciprocating motion with Si_3N_4 balls as counterparts. The sliding conditions were a load of 10 N, speed of 75 m/min, and duration of 30 minutes. The tests were conducted in three environments: dry, artificial seawater, and engine oil. The results indicate that the circle pattern performs better in dry conditions, while the grid pattern exhibits enhanced wear resistance by 75% in oil environments compared to dry conditions. Therefore, the geometrical pattern created by laser texturing has a significant impact on the tribological performance of Ti6Al4V material under various sliding conditions. These findings could have potential implications for improving the wear and frictional behavior of Ti6Al4V in different environments.

Received 27 July 2023; received in revised form 10 October 2023; accepted 14 December 2023.
To cite this article: Zul et al., (2024). Effect of multi-geometrical laser pattern of Ti6Al4V on frictional wear behaviour. Jurnal Tribologi 40, pp.78-94.

1.0 INTRODUCTION

Titanium alloys, particularly Ti6Al4V, have gained significant attention in various industries such as aerospace, automotive, biomedical, and chemical industries, due to its superior mechanical qualities, high strength-to-weight ratio, and good corrosion resistance (Ahuir-Torres et al., 2018). However, despite their numerous advantages, Ti6Al4V alloys are not exempt from wear-related challenges, which can limit their performance and durability such as failure of critical components and can cause severe destruction and loss of life (Pan et al., 2022). Therefore, there is a need to develop techniques that can effectively overcome wear problems associated with Ti6Al4V.

Frictional wear, a common phenomenon in sliding contact applications, poses a significant challenge for Ti6Al4V materials. Wear is characterized by the progressive loss of material from the surface due to mechanical interaction and can lead to reduced component lifespan, increased maintenance costs, and compromised functionality (Gao et al., 2012). Addressing wear-related issues is crucial for improving the reliability and longevity of Ti6Al4V components. The study of frictional wear behavior encompasses understanding the mechanisms involved and identifying effective strategies to mitigate wear-related problems (Ananth & Ramesh, 2015). Wear sliding tests, such as pin-on-disc or ball-on-disc tests, are widely employed to evaluate the wear characteristics of materials. These tests involve subjecting a sample to sliding contact with a counter face while monitoring wear rate, coefficient of friction, and surface morphology changes.

Laser texturing has emerged as a promising surface modification technique for enhancing the wear resistance of materials. Recent research on laser surface texturing (LST) has demonstrated its potential in enhancing the surface properties of metallic alloys. Yuan et al. (2019) investigated the effect of LST on the tribological behavior of a double glow plasma surface zirconizing coating on Ti6Al4V alloy, revealing improved wear resistance and friction coefficient of the zirconizing coating. The Ti6Al4V alloy's wear resistance was improved by the combination of the double glow plasma zirconizing technique and laser surface texturing; the textured specimens with a texture density of 5% showed the lowest mass loss values and the wear rate dropped by 20% and 26.6% percent in comparison to the TC4 alloy and Zr-coating without dimple texture on their surfaces. Cui et al. (2022) developed a biomimetic bilayer coating on laser textured Ti6Al4V alloy, which exhibited better wear resistance when lubricated in deionized water and different physiological solutions for long-term friction. The lowest friction coefficient was measured in a phosphate buffer (PBS) solution. Liang et al. (2018) studied the wear behavior of micro-grooved texture on WC-Ni3Al cermet, finding that the better wear resistance of the micro-groove on WC-10Ni3Al cermet came from the combined impacts of substantially slower WC grain development during laser machining and slower element diffusion during the sliding friction process. Additionally, Song et al. (2023) observed reduced friction and enhanced wear resistance in Ti6Al4V alloys through groove-textured surfaces using a combination of laser and abrasive belt texturing. Collectively, these studies highlight the versatility of LST as a surface modification technique for improving the properties of metallic alloys, with potential applications in various industries and fields. Further research in this area is crucial to optimize and expand the applications of LST in materials engineering and manufacturing industries.

Moreover, laser texturing techniques have enabled precise control over pattern geometry, density, and depth, offering new possibilities for enhancing wear performance (Roduan et al., 2020). Multi-geometrical patterns by laser texturing, including dimples, grooves, and channels, have shown significant potential in improving the tribological properties of materials. Seid Ahmed et al. (2021) investigated the LST of austenitic stainless steel, resulting in enhanced surface

hardness and wear resistance. In comparison to the untextured surface, the textured surfaces showed a reduced coefficient of friction and better wear resistance. The friction coefficient was reduced by up to 68% and the wear rate was reduced by 50% using the square pattern by laser texturing. The wear rate of perpendicular, parallel, and square samples was respectively reduced by about 22%, 37%, and 50% compared to the smooth surface. However, the studies of the patterns are limited as the study primarily focused on the parametric value of laser parameters and did not explore the effect of multi-geometrical surface textured wear properties.

Therefore, the current research aims to contribute to the understanding of the effect of multi-geometrical laser patterns on the frictional wear behavior of Ti6Al4V. By systematically analyzing the wear characteristics of Ti6Al4V samples with different laser patterns, this study seeks to provide valuable insights into the relationship between laser texturing, wear performance, and surface characteristics. The findings from this research will contribute to the development of optimized laser texturing techniques and guidelines for enhancing the wear resistance of Ti6Al4V alloys for more reliable and durable Ti6Al4V components in industries such as aerospace, automotive, and biomedical.

2.0 EXPERIMENTAL PROCEDURE

2.1 Materials and Preparation

In this study, Ti6Al4V samples (manufactured by Nippon Steel) with dimensions of 65mm x 15mm and a thickness of 1.2mm were prepared for subsequent testing and analysis. The chemical composition of the sample is shown in Table 1. To achieve the desired surface finish, a sequential polishing process was performed on the samples. Initially, rough polishing was carried out using 240, 400, 800, and 1,200 grit SiC abrasive paper to remove surface imperfections, eliminate residual scratches and refine the surface before undergoing the polishing process until a mirror-like surface finish.

Table 1: Chemical composition of Ti6Al4V.

Sample	**Chemical composition (wt%)**				
Ti-alloy Grade 5	Ti	Al	V	O	C
	87.45	5.25	4.62	1.76	0.92

2.2 Laser Texturing (LT)

LT process was used to fabricate multi-geometrical by using a Herolaser Marking system, which is equipped with an IPG Photonics Corp. (from the UK) 30W Ytterbium Fiber laser in a Q-switched mode. The laser operation with a 30μm focused laser beam diameter at a wavelength of 1064 nm and 100ns pulse width. The laser parameters were used as displayed in Table 2. Three samples were produced using three types of geometrical patterns: grid-array (sample A); circle-array (sample B); and triangular (sample C), with the details of each hatches line distance as shown in Figure 1.

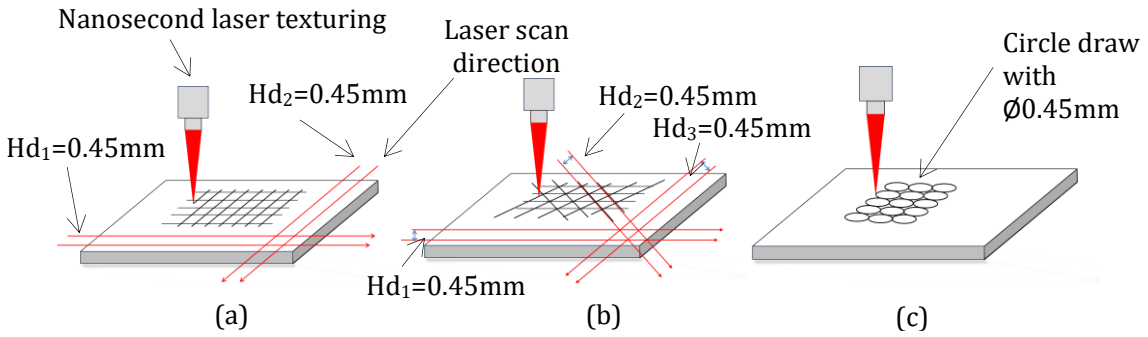

Figure 1: The laser texturing process for various geometrical patterns. (a) grid-array pattern with 2 angle hatches and 0.45mm each hatches line distance; (b) triangular shapes with 3 different hatches angles and 0.45mm each hatches line distance; and (c) Circle-array with single laser direction following the circle draws. All the geometrical patterns are close loop patterns with 0.45mm distances between hatches, except for the circle pattern is 0.45mm in diameter.

Table 2: The process parameters and multi-geometrical pattern of laser texturing on Ti6Al4V.

Laser parameter	**Unit**	**Value**
Laser power	W	18
Laser frequency	kHz	40
Laser speed	mm/s	220
Pattern texture		Grid-array, Triangular, Circle-array
Environment		Argon

2.3 Mechanical Properties

The surface hardness test was performed using Vickers Hardness Tester (FV-310, Future Tech). The Vickers hardness (HV) was obtained from (1):

$$HV = 0.1891 \times \frac{P}{d^2} \quad (1)$$

where P is the test load on the diamond indentation (g), and d is the measurement diagonal length of the pyramidal indentation on the sample surface (μm). As shown in Figure 2, a total of 15 measurements were made in various places with the test load for the indentation was 100N with a dwell time of 15 s.

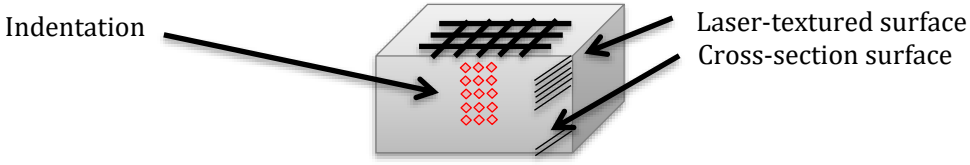

Figure 2: multi-geometrical pattern by nanosecond laser texturing. (a) Grid-array; (b) triangular-array; and (c) circle-array.

2.3 Frictional Wear Sliding Test

The study of the sliding wear and friction behaviour was performed using Ducom TR-20 ball-on-flat tribometer. The Si_3N_4 ball with a 10mm diameter as counterface was slid on the multi-geometrical textured surface samples with a fixed load of 10N for the duration of 1,800s at a speed of 75 m/min. The test was carried out in dry, artificial seawater (SW), and oily conditions. To determine the weight loss of each sample, Shimadzu (AUW220D) digital electronic balancer measurements were taken before and after the test with a decimal place of 0.01 mg accuracy. The volume loss was then calculated by dividing the weight loss by the specific density. The specific wear rate, WR was calculated according to Archard's wear (2) (Archard, 1953) as shown below:

$$WR = \frac{m_{loss}}{\rho F_n D} \tag{2}$$

where m_{loss} is the volume loss, F_n is the applied load and D is the sliding distance. Winducom 2010 was used to record the friction forces and coefficient of friction (COF) of the samples during the wear test. The average COF was determined using the collected data. The average value of the wear tests performed twice on each sample is presented.

2.4 Surface Characterization

The surface composition of the sample was observed under the floor-top Scanning Electron Microscope (SEM) with Energy Dispersive X-Ray Spectroscopy (EDX), model JEOL JSM-IT200 (from Japan). The laser textured surface and worn surface after the wear sliding test was analyzed via a 3D measuring laser microscope (Olympus LEXT OLS5000). The areal surface roughness Sa and Sq was determined on the whole sample surface with an optical magnification of 10x was used, leading to a scan area of 853 x 853 µm. The shape profile parameter of the textured surface was determined by measuring 2D cross-sectional profiles of each sample, as depicted in Figure 4, to assess the crater profile.

3.0 RESULTS AND DISCUSSION

3.1 Surface Topographical Properties

Figure 3 explores the effects of laser beam treatment on three surface patterns: grid array, triangular, and circle array. The grid array pattern consists of intersecting grooves, the triangular pattern features triangular grooves the circle array pattern comprises closely spaced circular craters.

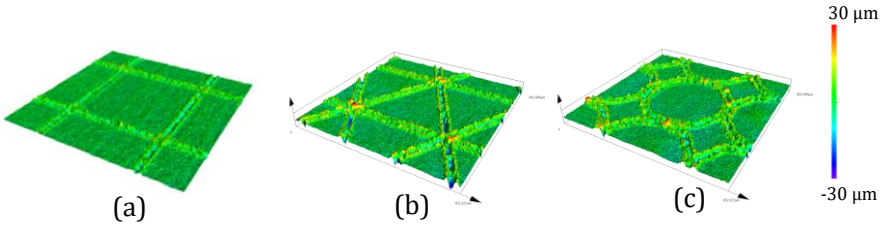

Figure 3: multi-geometrical pattern by nanosecond laser texturing. (a) Grid-array; (b) triangular-array; and (c) circle-array.

The surface profile parameters were measured using three key metrics (refer to Figure 4): the diameter of the crater (D) to quantify the size of the surface features, the height (h) of the crater from the valley to the peak provides insights into the depth or elevation difference between the lowest point (valley) and the highest point (peak) of the surface, and the (c) is the center between two grooves assists in determining the spacing and alignment of surface patterns. These parameters provide essential information about the surface roughness factor or area ratio (r_w) by a previous study from Jain et al. (Jain & Bajpai, 2022) as per Equation (3):

$$r_w = \frac{c^2 + \pi Dh}{c^2} \tag{3}$$

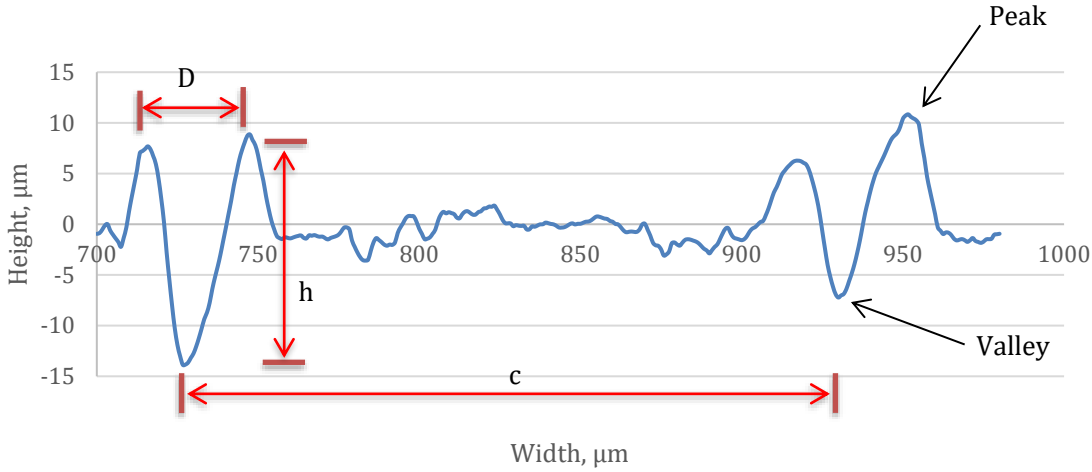

Figure 4: The surface textured profile is based on 3 parameters of c, D, and h.

The results of r_w in Figure 5 indicate that variations in the values of c, D, and h have a minor effect on the overall surface roughness. Although there are slight differences in the calculated r_w values among the textures, the increase in roughness factor is relatively small about 0.3% compared of the lowest (triangular-array) and the highest (circle-array). This suggests that the specific geometric characteristics of the surface, such as the arrangement of grooves and the size of craters, have a minimal impact on the overall roughness factor. Other factors, such as the texture's density and spacing, may also play a role in influencing surface roughness (W. Wang et al., 2021).

Different surface patterns, such as circular, triangular, or grid arrays, can lead to variations in the values of c, D, and h, even when using the same laser parameters. The pattern design itself, including the spacing between grooves or the arrangement of craters, can influence the center (c) and diameter (D) values. Additionally, the material response to the laser beam, influenced by factors like composition and thermal conductivity (Li et al., 2020), can cause variations in the height (h) of the craters or the depth of material removal (Y. Wang et al., 2020). Furthermore, the interaction of the laser beam with existing surface features, such as roughness or microstructures, can also impact c, D, and h (Dowding & Borman, 2015). These factors highlight how different surface patterns can result in variations in the surface roughness parameters when subjected to laser processing.

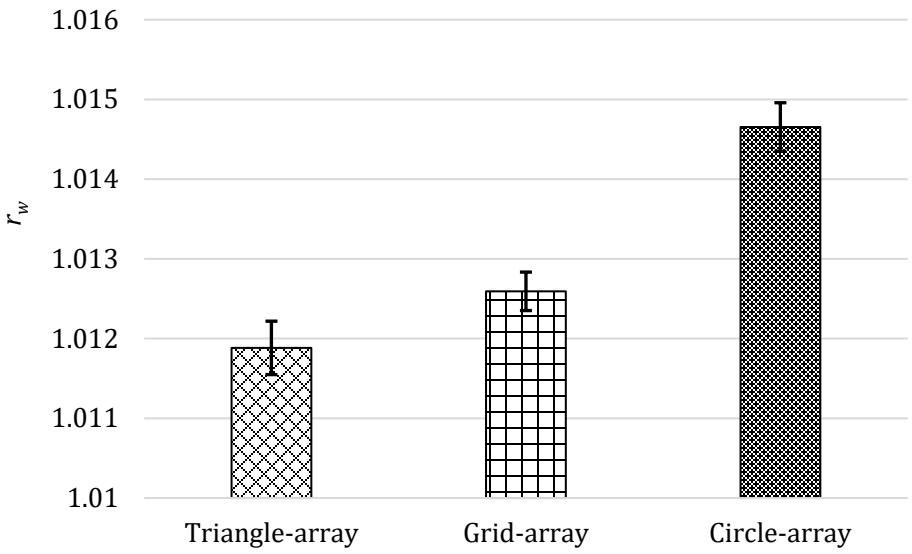

Figure 5: Texture density of different geometry by laser texturing.

Evaluating surface texture through 3D areal analysis offers greater possibilities compared to the examination of 2D profiles. The assessment of surface topography, which constitutes a three-dimensional analysis on micro or nanoscales, holds significant relevance across various scientific and practical domains (Pawlus et al., 2021). Among the multitude of texture parameters, those associated with height are frequently employed. Figure 6 shows the results of Sa (arithmetic mean deviation) and Sq (root-mean-square deviation of surface) for three different surface geometrical laser textured (Zeng et al., 2018). According to Jansons et al. (2022), the most typical amplitude parameters which are used in surface characterization such as Sa and Sq, usually used to characterize the surface texture, and at the same time, indirectly may affect the surface contact, lubrication, friction and wear.

The circle-array texture and the triangular pattern exhibit moderate roughness. On the other hand, the grid-array texture demonstrates the lowest roughness. The results suggest that the grid-array texture provides the smoothest surface among the three, while the circle-array and triangular textures exhibit slightly higher roughness. The choice of texture depends on the specific requirements of the application, considering factors such as desired surface features and the desired balance between smoothness and other performance characteristics.

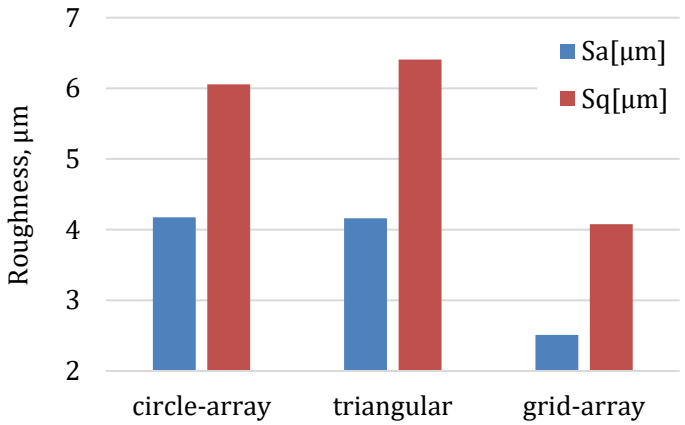

Figure 6: Surface areal roughness distribution of multi-geometrical laser-textured surface.

3.2 Surface Morphology

SEM-EDX results for the samples after laser texturing indicate the variations in the elemental composition between different spots within the same sample and among different samples as displayed in Figure 7. These SEM-EDX results provide insights into the elemental composition of the analyzed samples. In the provided SEM-EDX results, the elements of interest related to oxidation and carbonization are Oxygen (O) and Carbon (C) which play significant roles in the surface composition and properties of materials.

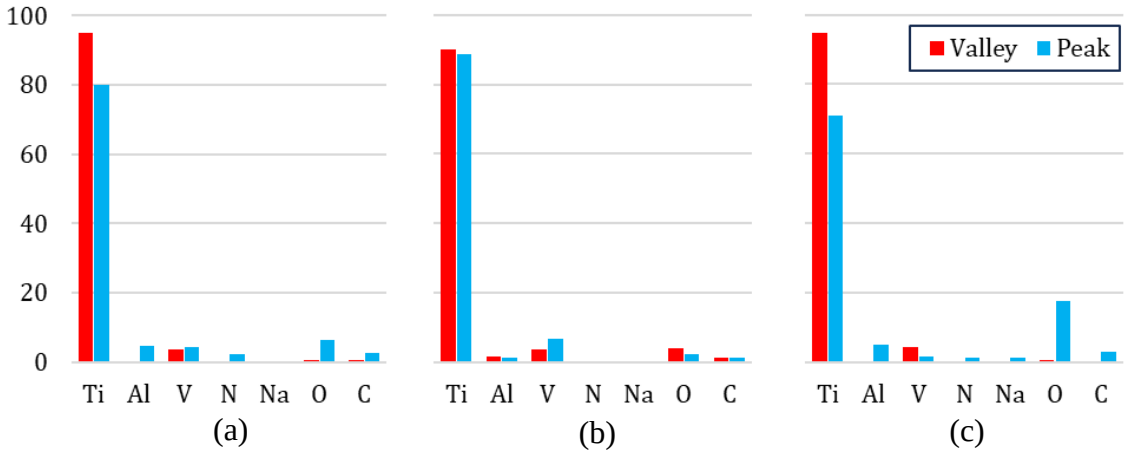

Figure 7: SEM-EDX results from the spot of peak and valley of (a) grid array, (b) triangular, and (c) circle array.

Increased levels of oxygen in a material indicate the occurrence of oxidation processes, resulting in the formation of oxide layers on the surface (Pohrelyuk et al., 2018). This can affect the material's properties, including hardness, corrosion resistance, and surface morphology. Oxidation can lead to surface degradation, such as increased roughness and reduced mechanical strength (Mao et al., 2020). However, the oxide layer can also act as a protective barrier against

further oxidation (Mukherjee et al., 2021). The presence of higher percentages of oxygen, as seen in Figure 8 for circle-array is at the peak spot, suggests a relatively higher level of oxidation compared to other samples.

Carbon exists in various forms and its presence is indicated by the percentage of C content (Figure 8) in the elemental composition obtained from SEM-EDX analysis. Carbonization involves the introduction of carbon or the formation of carbon-based compounds on the material's surface. Carbon can originate from different sources such as organic contamination, carbon-based coatings, or intentional carbonization treatments. The presence of carbon, as observed in the analyzed samples, suggests the occurrence of carbonization or the presence of carbon-containing compounds. In this case, the carbon content is present from the cleaning process by using an ultrasonic bath in ethanol after laser texturing (Y. Wang et al., 2020). After cleaning, a fascinating phenomenon emerged—the adsorption of organic groups from the ambient air. The study from Schnell et al. (2020) found that the increase in carbon content, rising from 29.5% to 32% within just 14 days. Cleaning the surface revealed atmospheric carbon-rich organic molecules replacing water and attaching to the surface's hydroxylic groups. This supports the notion that structured surfaces are hydroxylated by coordinatively unsaturated metal ions reacting with water to bind airborne hydrocarbons (Jagdheesh et al., 2019). Even structured surfaces cleansed with pure water or acetone showed reactivity after cleaning, adsorbing organic molecules as carbon groups increased (Schnell et al., 2020). Carbonization can enhance the mechanical properties of materials, particularly hardness and wear resistance, by forming hard carbonaceous phases or carbides (Xiao et al., 2020). Carbon-based coatings can also provide protective layers against wear, friction, and corrosion.

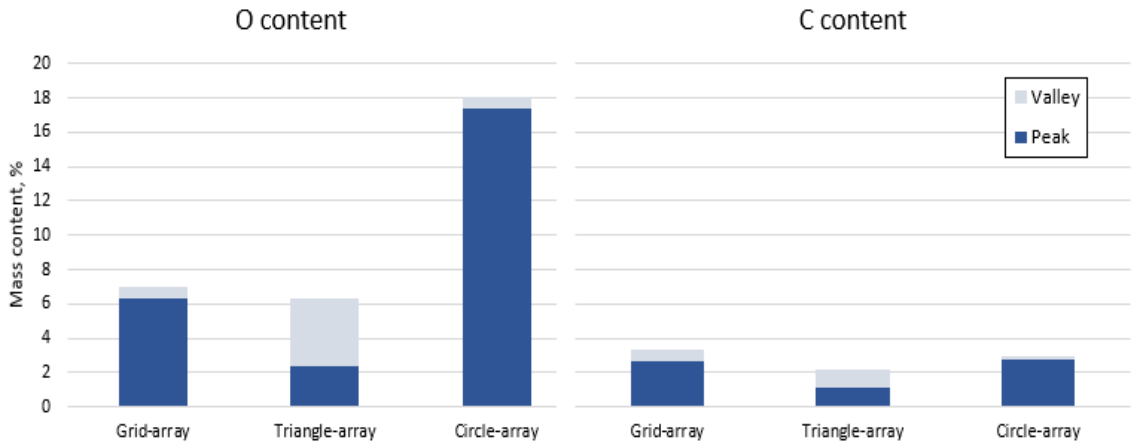

Figure 8: SEM-EDX results from the spot of peak and valley of (a) grid array, (b) triangular, and (c) circle array.

3.3 Surface Microhardness

Figure 9 compares the distances and corresponding hardness values (HVN) for both untextured and laser-textured surfaces. For the untextured surface, the hardness values significantly decrease from ~330 HV_1 to ~300 HV_1. On the other hand, for the laser-textured surface, the hardness values consistently range from ~325 HV_1 to ~315 HV_1. Hardness changes from laser surface treatment are closely linked to cooling phase transformations (Menci et al., 2019; Xu et al., 2019). At high temperatures, the β-phase becomes the hard, brittle martensitic α-phase and the ω-phase is created (Omoniyi et al., 2021). A martensitic α-phase is observed after the alpha-phase becomes a beta-phase and cooling occurs rapidly (Guo & Jonas, 2021). Hardness measurements in the β-phase often show lower values than those in the α-phase (Geng et al., 2020). Surface hardness during laser treatment is greatly influenced by the production of the martensitic phase, as well as elements like the presence of martensitic plates and smaller grains. This increases post-treatment hardness values with some variances (Dai et al., 2020).

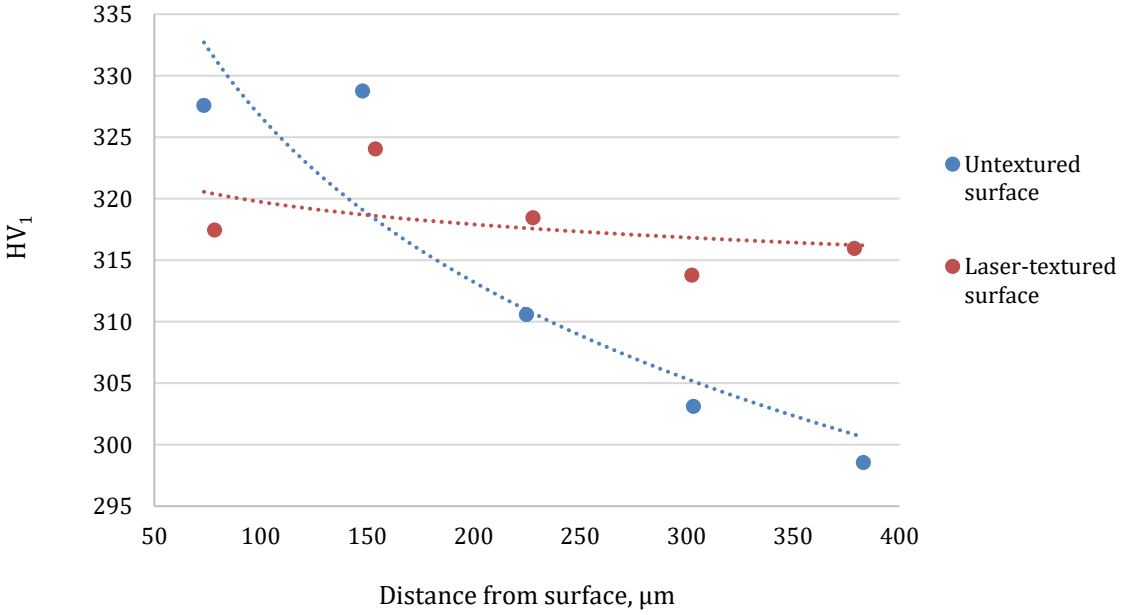

Figure 9: Cross-sectional microhardness value for untextured and laser-textured surface.

3.4 Surface Wear Performance

Figure 10 shows the wear rate and COF of all samples including an untextured surface under three testing conditions. All the samples show almost similar WR results in dry conditions. However, the grid pattern achieves a better wear rate compared to the other patterns under fluidity conditions. This is due to the grid pattern's enhanced lubrication, which is facilitated by the grooves that allow for improved fluid flow and distribution of the lubricant across the sliding interface (Gachot et al., 2017). The reduced contact area of the grid pattern also contributes to lower wear rates by minimizing direct contact between the surfaces (Chang et al., 2015). Additionally, the grooves promote the formation of a protective tribofilm and aid in the removal

of wear debris, further reducing friction and wear (Khaemba et al., 2020). These factors collectively make the grid pattern more effective in achieving a better wear rate.

The influence of fluid flow within pattern channels on wear rates is evident in varying conditions. In seawater, the grid pattern's grooves effectively remove corrosive elements (Kumari et al., 2019), resulting in decreased wear rates. In oil lubrication, these grooves aid oil distribution and the creation of a stable lubricating film, reducing direct contact and friction. These flow dynamics contribute to the grid pattern achieving superior wear rates in both seawater and oil conditions (Conradi et al., 2021). The differences between the triangular and circle array patterns are not explicitly mentioned in the provided data. However, in general, the triangular array pattern may have some similarities to the grid pattern in terms of enhanced lubrication and reduced contact area (Singh et al., 2019), although the specific geometric features and arrangement of the triangles may influence the fluid flow and wear behavior differently. The circle array pattern, on the other hand, may have a less effective fluid flow and lubrication due to the absence of grooves or channels, resulting in higher wear rates compared to the grid pattern (Lu & Wood, 2020).

In conclusion, considering the dynamics of fluid flow and the potential for better lubrication conditions, the grid array pattern is likely to be more favorable. Its grooved design allows for improved fluid distribution, which can enhance the formation of a stable and uniform lubricating film. This, in turn, helps to reduce direct contact and friction between the sliding surfaces, leading to better lubrication and potentially lower wear rates.

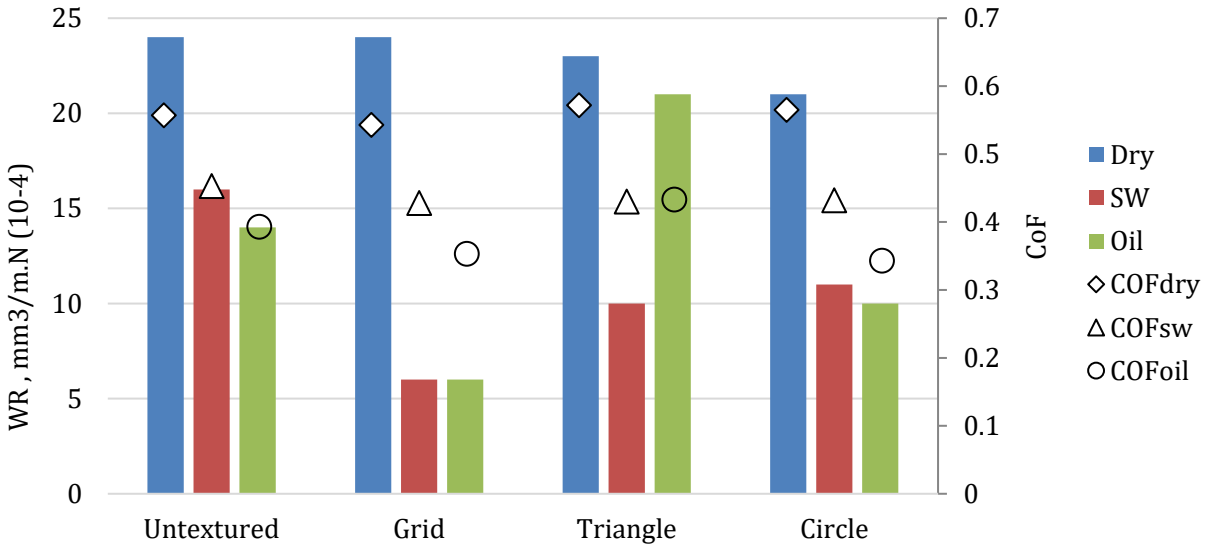

Figure 10: Wear rate and COF of the multi-geometrical laser-textured surface.

For a clearer understanding, the wear graph for the wear test under oil conditions is shown in Figure 11. Circle and grid arrays perform in smooth sliding conditions when compared to triangular. However, the grid array pattern exhibits enhanced wear resistance by 71% and 40%

in oil testing conditions compared to triangle and circle pattern, respectively. This is because of the effect of O and C increase in peak, which is shown in Figure 7. The relationship between the presence and increasing carbon (C) element and the better wear rate (WR) observed in the grid and circle array patterns compared to the triangular pattern can be related to the results obtained from the previous SEM-EDX analysis. The SEM-EDX analysis provided information on the elemental composition of the samples, including the oxide and carbon content.

Based on the results, it can be inferred that the grid and circle array patterns exhibited higher carbon percentages compared to the triangular pattern. The higher carbon content in the grid and circle array patterns can be attributed to factors such as the laser texturing process or the design and arrangement of the patterns, which influence carbon incorporation. The increased carbon content in the grid and circle array patterns contributes to enhanced wear resistance by forming protective carbonaceous phases or carbides on the surface. This protective layer reduces wear between the mating surfaces and results in a lower wear rate compared to the triangular pattern, which may have had a relatively lower carbon content. Thus, the SEM-EDX results provide insights into the carbon distribution and its relationship to the improved wear rate observed in the grid and circle array patterns.

It is also worth noting that the friction surfaces of tribological pairs show evident indicators of an oxidation wear mechanism, as seen by the higher oxygen content on the laser-textured surface (Philip et al., 2019). This result implies that the initial oxide film on the metal surface is removed during friction as the hard asperities come into contact with the high points of the oxide layer, revealing the underlying metal. Following that, the exposed metal immediately reacts with the oxygen in the surrounding air, generating a new oxide layer that is scraped off in succeeding cycles by the interacting asperities (Pohrelyuk et al., 2018).

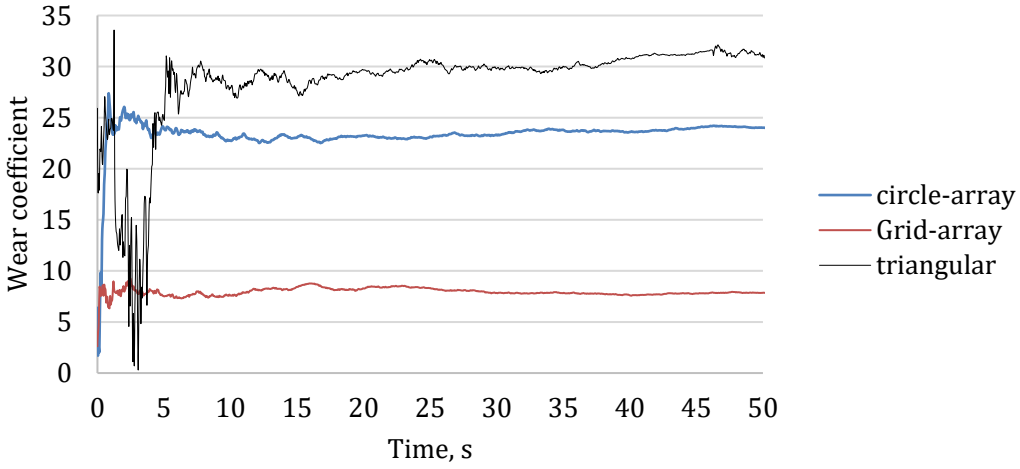

Figure 11: wear coefficient on oil sliding condition.

The condition of frictional wear behaviour is closely related to the worn surface profile as shown in Figure 12. The width of the wear track for the grid array is shorter than the circle array indicating that the grid array pattern, with its intersecting grooves, provides channels for the oil to flow and distribute more effectively within the contact area. This promotes better lubrication

and reduces frictional heat generation (Mao et al., 2020). On the other hand, the circular surface of the circle-array pattern lacks such channels, potentially leading to less efficient oil distribution.

In the wear sliding test conducted under oil conditions, the presence of lubricating oil between the sliding surfaces plays a crucial role. The oil forms a thin film that acts as a barrier between the mating surfaces, reducing direct contact and friction. This lubricating film helps to minimize wear and prevent excessive material removal.

Moreover, the grid array pattern, with its channels and grooves, allows for better retention and distribution of the lubricating oil within the contact area. This results in the formation of a more uniform and thicker oil film between the sliding surfaces. The thicker oil film provides improved lubrication, reducing direct contact and wear between the surfaces.

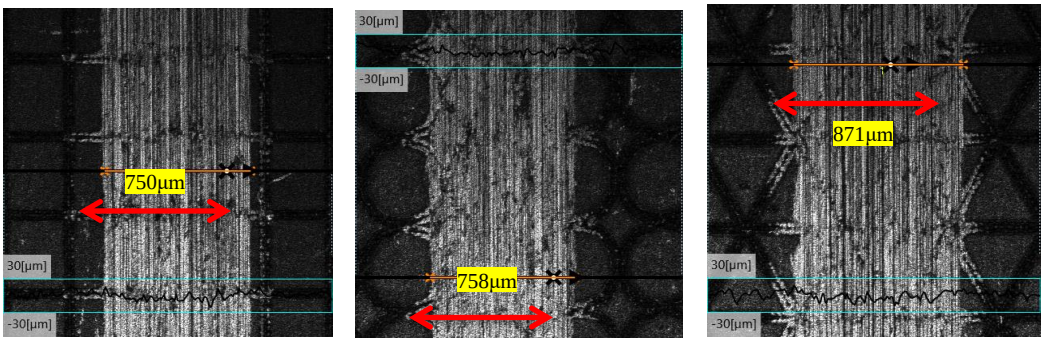

(a) (b) (c)

Figure 12: The intensity images of the width of the wear track for (a) grid-array, (b) circle-array, and (c) triangle-array, on wear sliding under oil conditions.

CONCLUSIONS

In this paper, the Ti6Al4V surface was fabricated by laser surface texturing with three patterns including grid array, triangular, and circle array pattern. The laser texturing process influenced the surface characteristics such as surface textured profile, roughness parameters and elemental composition. The multi-geometrical laser textured surface undergoes a wear sliding test to analyze the wear performance. The conclusion that can be drawn from this study are:

a) The grid pattern exhibited the lowest wear rate among the studied patterns, indicating its superior performance in reducing material loss and surface degradation compared to the triangular and circle array patterns.
b) The higher carbon content observed in the grid and circle array patterns, as indicated by SEM-EDX analysis, suggests a relationship between increased carbon incorporation and improved wear resistance. The formation of protective carbonaceous phases or carbides on the surface contributes to reduced wear rates in these patterns.
c) The presence of grooves in the grid pattern facilitates fluid flow and effective lubrication, leading to lower friction and wear. This effect is particularly significant in seawater and oil conditions, where the grid pattern demonstrated 75% better wear performance compared to other patterns.

Overall, this study highlights the importance of surface pattern design, carbon incorporation, fluid flow, and lubrication in influencing wear resistance. The findings contribute to a better

understanding of how laser-textured patterns can be optimized to enhance the performance and durability of materials in various operating conditions.

ACKNOWLEDGMENTS

Universiti Malaysia Pahang Flagship Grant (PDU213002-1) and Universiti Malaysia Pahang Postgraduate Research Scheme (PGRS200302)

REFERENCES

Ahuir-Torres, J. I., Arenas, M. A., Perrie, W., & de Damborenea, J. (2018). Influence of laser parameters in surface texturing of Ti6Al4V and AA2024-T3 alloys. Optics and Lasers in Engineering, 103(December 2017), 100–109. https://doi.org/10.1016/j.optlaseng.2017.12.004

Ananth, M. P., & Ramesh, R. (2015). Reciprocating Sliding Wear Performance of Hard Coating on Modified Titanium Alloy Surfaces. Tribology Transactions, 58(1), 169–176. https://doi.org/10.1080/10402004.2014.943338

Archard, J. F. (1953). Contact and rubbing of flat surfaces. Journal of Applied Physics, 24(8). https://doi.org/10.1063/1.1721448

Chang, B. P., Akil, H. M., & Nasir, R. B. M. (2015). Dry sliding wear behaviour of talc-reinforced UHMWPE composite for implant application. Sains Malaysiana, 44(6), 819–825. https://doi.org/10.17576/jsm-2015-4406-07

Conradi, M., Kocijan, A., Klobčar, D., & Podgornik, B. (2021). Tribological response of laser-textured Ti6Al4V alloy under dry conditions and lubricated with Hank's solution. Tribology International, 160(December 2020). https://doi.org/10.1016/j.triboint.2021.107049

Cui, L., Li, H., Gong, C., Huang, J., & Xiong, D. (2022). A biomimetic bilayer coating on laser-textured Ti6Al4V alloy with excellent surface wettability and biotribological properties for artificial joints. Ceramics International, 48(18), 26264–26273. https://doi.org/10.1016/J.CERAMINT.2022.05.309

Dai, J., Wang, T., Chai, L., Hu, X., Zhang, L., & Guo, N. (2020). Characterization and correlation of microstructure and hardness of Ti–6Al–4V sheet surface-treated by pulsed laser. Journal of Alloys and Compounds, 826, 154243. https://doi.org/10.1016/j.jallcom.2020.154243

Dowding, C., & Borman, A. (2015). Laser-initiated ablation of materials. Laser Surface Engineering: Processes and Applications, 523–546. https://doi.org/10.1016/B978-1-78242-074-3.00022-2

Gachot, C., Rosenkranz, A., Hsu, S. M., & Costa, H. L. (2017). A critical assessment of surface texturing for friction and wear improvement. Wear, 372–373, 21–41. https://doi.org/10.1016/j.wear.2016.11.020

Gao, N., Wang, C. T., Wood, R. J. K., & Langdon, T. G. (2012). Tribological properties of ultrafine-grained materials processed by severe plastic deformation. Journal of Materials Science, 47(12), 4779–4797. https://doi.org/10.1007/s10853-011-6231-z

Geng, Y., McCarthy, É., Brabazon, D., & Harrison, N. (2020). Ti6Al4V functionally graded material via high power and high speed laser surface modification. Surface and Coatings Technology, 398(June). https://doi.org/10.1016/j.surfcoat.2020.126085

Guo, B., & Jonas, J. J. (2021). Dynamic transformation during the high temperature deformation of titanium alloys. Journal of Alloys and Compounds, 884, 161179. https://doi.org/10.1016/j.jallcom.2021.161179

Jagdheesh, R., Diaz, M., Marimuthu, S., & Ocaña, J. L. (2019). Hybrid laser and vacuum process for rapid ultrahydrophobic Ti-6Al-4 V surface formation. Applied Surface Science, 471(November 2018), 759–766. https://doi.org/10.1016/j.apsusc.2018.12.047

Jain, A., & Bajpai, V. (2022). Alteration in Ti6Al4V implant surface properties with micro textures density. Surface Engineering, 38(2), 174–182. https://doi.org/10.1080/02670844.2022.2058163

Jansons, E., Lungevics, J., Kanders, U., Leitans, A., Civcisa, G., Linins, O., Kundzins, K., & Boiko, I. (2022). Tribological and Mechanical Properties of the Nanostructured Superlattice Coatings with Respect to Surface Texture. Lubricants, 10(11). https://doi.org/10.3390/lubricants10110285

Khaemba, D. N., Azam, A., See, T. L., Neville, A., & Salehi, F. M. (2020). Understanding the role of surface textures in improving the performance of boundary additives, part I: Experimental. Tribology International, 146(January), 106243. https://doi.org/10.1016/j.triboint.2020.106243

Kumari, R., Pfleging, W., Besser, H., & Majumdar, J. D. (2019). Microstructure and corrosion behavior of laser induced periodic patterned titanium based alloy. Optics and Laser Technology, 116(July 2018), 196–213. https://doi.org/10.1016/j.optlastec.2019.03.017

Li, Z., Chen, N., Li, L., Wu, Y., & He, N. (2020). Influence of the grain size of CVD diamond on the thermal conductivity, material removal depth and surface roughness in nanosecond laser machining. In Ceramics International (Vol. 46, Issue 12). Techna Group S.r.l. https://doi.org/10.1016/j.ceramint.2020.05.157

Liang, L., Yuan, J., Li, X., Yang, F., & Jiang, L. (2018). Wear behavior of the micro-grooved texture on WC-Ni3Al cermet prepared by laser surface texturing. International Journal of Refractory Metals and Hard Materials, 72(December 2017), 211–222. https://doi.org/10.1016/j.ijrmhm.2017.12.023

Lu, P., & Wood, R. J. K. (2020). Tribological performance of surface texturing in mechanical applications-a review. Surface Topography: Metrology and Properties, 8(4). https://doi.org/10.1088/2051-672X/abb6d0

Mao, B., Siddaiah, A., Liao, Y., & Menezes, P. L. (2020). Laser surface texturing and related techniques for enhancing tribological performance of engineering materials: A review. Journal of Manufacturing Processes, 53(December 2019), 153–173. https://doi.org/10.1016/j.jmapro.2020.02.009

Menci, G., Demir, A. G., Waugh, D. G., Lawrence, J., & Previtali, B. (2019). Laser surface texturing of β-Ti alloy for orthopaedics: Effect of different wavelengths and pulse durations. Applied Surface Science, 489(April), 175–186. https://doi.org/10.1016/j.apsusc.2019.05.111

Mukherjee, S., Dhara, S., & Saha, P. (2021). Enhanced corrosion, tribocorrosion resistance and controllable osteogenic potential of stem cells on micro-rippled Ti6Al4V surfaces produced by pulsed laser remelting. Journal of Manufacturing Processes, 65(July 2020), 119–133. https://doi.org/10.1016/j.jmapro.2021.03.023

Omoniyi, P. O., Akinlabi, E. T., & Mahamood, R. M. (2021). Heat Treatments of Ti6Al4V Alloys for Industrial Applications: An Overview. IOP Conference Series: Materials Science and Engineering, 1107(1), 012094. https://doi.org/10.1088/1757-899x/1107/1/012094

Pan, X., He, W., Cai, Z., Wang, X., Liu, P., Luo, S., & Zhou, L. (2022). Investigations on femtosecond laser-induced surface modification and periodic micropatterning with anti-friction properties on Ti6Al4V titanium alloy. Chinese Journal of Aeronautics, 35(4), 521–537. https://doi.org/10.1016/j.cja.2021.01.003

Pawlus, P., Reizer, R., & Wieczorowski, M. (2021). Functional importance of surface texture parameters. Materials, 14(18), 1–29. https://doi.org/10.3390/ma14185326

Philip, J. T., Mathew, J., & Kuriachen, B. (2019). Tribology of Ti6Al4V: A review. Friction, 7(6), 497–536. https://doi.org/10.1007/s40544-019-0338-7

Pohrelyuk, I. M., Sheykin, S. E., Padgurskas, J., & Lavrys, S. M. (2018). Wear resistance of two-phase titanium alloy after deformation-diffusion treatment. Tribology International, 127(March), 404–411. https://doi.org/10.1016/j.triboint.2018.06.011

Roduan, S. F., Wahab, J. A., Mohd Salleh, M. A. A., Mohd Mahayuddin, N. A. H., Halil, A. M., & Ishak, M. (2020). Effect of LST parameter on surface morphology of modified copper substrates. Jurnal Tribologi, 26(July), 84–91.

Schnell, G., Polley, C., Bartling, S., & Seitz, H. (2020). Effect of chemical solvents on the wetting behavior over time of femtosecond laser structured ti6al4v surfaces. Nanomaterials, 10(6), 1–20. https://doi.org/10.3390/NANO10061241

Seid Ahmed, Y., M. DePaiva, J., L. Amorim, F., D. Torres, R., de Rossi, W., & C. Veldhuis, S. (2021). Laser surface texturing and characterization of austenitic stainless steel for the improvement of its surface properties. International Journal of Advanced Manufacturing Technology, 115(5–6), 1795–1808. https://doi.org/10.1007/s00170-021-07284-z

Singh, A., Patel, D. S., Ramkumar, J., & Balani, K. (2019). Single step laser surface texturing for enhancing contact angle and tribological properties. International Journal of Advanced Manufacturing Technology, 100(5–8), 1253–1267. https://doi.org/10.1007/s00170-018-1579-8

Song, S., Xiao, G., Liu, Y., Zhou, K., Liu, S., & Huang, J. (2023). Tribological response of groove-textured surface with compressive stress on Ti6Al4V processed by laser and abrasive belt. Tribology International, 180(174), 108265. https://doi.org/10.1016/j.triboint.2023.108265

Wang, W., Liu, Z., Chen, D., Xie, Z., & Song, J. (2021). Influence of Different Surface Texture Parameters on the Contact Performance of Piston Ring-Sleeve Friction Pair of Hydraulic Cylinders. Advances in Materials Science and Engineering, 2021. https://doi.org/10.1155/2021/5495995

Wang, Y., Zhao, X., Ke, C., Yu, J., & Wang, R. (2020). Nanosecond laser fabrication of superhydrophobic Ti6Al4V surfaces assisted with different liquids. Colloids and Interface Science Communications, 35(December 2019), 100256. https://doi.org/10.1016/j.colcom.2020.100256

Xiao, J.-K., Tan, H., Chen, J., Martini, A., & Zhang, C. (2020). Effect of carbon content on microstructure, hardness and wear resistance of CoCrFeMnNiCx high-entropy alloys. Journal of Alloys and Compounds, 847, 156533. https://doi.org/https://doi.org/10.1016/j.jallcom.2020.156533

Xu, Y., Li, Z., Zhang, G., Wang, G., Zeng, Z., Wang, C., Wang, C., Zhao, S., Zhang, Y., & Ren, T. (2019). Electrochemical corrosion and anisotropic tribological properties of bioinspired hierarchical morphologies on Ti-6Al-4V fabricated by laser texturing. Tribology International, 134. https://doi.org/10.1016/j.triboint.2019.01.040

Yuan, S., Lin, N., Zou, J., Liu, Z., Wang, Z., Tian, L., Qin, L., Zhang, H., Wang, Z., Tang, B., & Wu, Y. (2019). Effect of laser surface texturing (LST) on tribological behavior of double glow plasma

surface zirconizing coating on Ti6Al4V alloy. Surface and Coatings Technology, 368(January), 97–109. https://doi.org/10.1016/j.surfcoat.2019.04.038

Zeng, Q., Qin, Y., Chang, W., & Luo, X. (2018). Correlating and evaluating the functionality-related properties with surface texture parameters and specific characteristics of machined components. International Journal of Mechanical Sciences, 149(July), 62–72. https://doi.org/10.1016/j.ijmecsci.2018.09.044